Performance of geotechnical seismic isolation system using rubber-soil mixtures in centrifuge testing

Tsang, Hing-Ho; Tran, Duc Phu; Hung, Wen Yi; Pitilakis, Kyriazis; Gad, Emad F.

Published in:
Earthquake Engineering and Structural Dynamics

DOI:
10.1002/eqe.3398

Publication date:
2021

Licence:
Other

Document Version
Peer reviewed version

PERFORMANCE OF GEOTECHNICAL SEISMIC ISOLATION SYSTEM USING RUBBER-SOIL MIXTURES IN CENTRIFUGE TESTING

Hing-Ho Tsang[1], Duc-Phu Tran[1], Wen-Yi Hung[2], Kyriazis Pitilakis[3], Emad F. Gad[1]

[1] School of Engineering, Swinburne University of Technology, Melbourne, Australia

[2] Department of Civil Engineering, National Central University, Taoyuan, Taiwan

[3] Department of Civil Engineering, Aristotle University, Thessaloniki, Greece

Correspondence

Hing-Ho Tsang, School of Engineering, Swinburne University of Technology, Melbourne, Australia
Email: htsang@swin.edu.au

SUMMARY

Geotechnical seismic isolation (GSI) system involves the dynamic interaction between structure and low-modulus foundation material, such as rubber-soil mixtures (RSM). Whilst numerical studies have been carried out to demonstrate the potential benefits of GSI-RSM system, experimental research is indispensable for confirming its isolation mechanism and effectiveness in reducing structural demand. In this regard, centrifuge modelling with an earthquake shaker under an acceleration field of 50 g adopted in this study can mimic the actual nonlinear dynamic response characteristics of RSM and subsoil in a coupled soil-foundation-structure system. This is the first time the performance of GSI-RSM system was examined in a geotechnical centrifuge. It was found that an average of 40–50% reduction of structural demand can be achieved. The increase in both the horizontal and rotation responses of the foundation was also evidenced. The unique augmented rocking mechanism with reversible foundation rotation was highlighted.

KEYWORDS

geotechnical seismic isolation, rubber-soil mixtures, waste tyre, centrifuge, augmented rocking mechanism

1 INTRODUCTION

Earthquake-resistant buildings and infrastructure are indispensable elements of safe and resilient cities. Geotechnical Seismic Isolation (GSI) system (named in Tsang 2009) is an emerging technology, which has attracted significant interest globally in the past decade, as briefly reviewed in Tsang and Pitilakis (2019). Rubber-soil mixtures (RSM) have firstly been proposed as a suitable foundation material for forming a low-stiffness isolation layer with controllable properties (Tsang 2008), which have been proven by numerous studies (e.g. Shimamura 2012; Tsang et al. 2012; Pitilakis et al. 2015; Brunet et al. 2016), whilst other materials such as expanded polystyrene (EPS) geofoam are currently being explored for similar purpose (Karatzia and Mylonakis 2017). Waste tyre rubber has been considered as a desirable candidate for making RSM (Tsang 2012), rendering GSI system an environmentally sound and low-cost technology that is affordable for the impoverished parts of the world, where earthquake disasters often exacerbate poverty (Xiong and Li 2013; Anbazhagan et al. 2016; Tsiavos et al. 2019). All these contribute to various United Nations Sustainable Development Goals (SDGs) in relation to resilient infrastructure and cities, sustainable resource consumption and waste management, as well as reduction of poverty and inequality.

The mechanism of GSI system has been explained and illustrated with the use of a lumped-parameter analytical model (Tsang and Pitilakis 2019). The “improved” foundation material reduces the lateral stiffness between the building and the subsoil, which serves as an isolation layer like a traditional base isolator. Moreover, the lower modulus of the foundation material reduces the rocking stiffness, which would increase the rotation response of the foundation. This is described as the augmented rocking mechanism that is illustrated by a schematic diagram in Fig. 1. Hence, the beneficial effects of soil-foundation-structure interaction can be exploited. Similar concepts have also been applied to

underground infrastructure (Tsang et al. 2009; Terzi et al. 2015) as well as retaining and bridge abutment structures (Lee et al. 1999; Hazarika et al. 2008; Xiao et al. 2012; Argyroudis et al. 2016; Mitoulis et al. 2016).

The augmented rocking mechanism is similar to the conventional rocking isolation (below foundation) based on natural or improved soil (e.g. Anastasopoulos et al. 2010; 2012; Gajan et al. 2005; 2008). For example, the shaking table test reported in Anastasopoulos et al. (2013) shows that the acceleration response of bridge deck designed with rocking isolation can be reduced by 50–60%. As GSI was defined in Tsang (2009) as an isolation technique that involves direct contact with geological sediments, rocking isolation (below foundation) can also be included into the family of GSI techniques. Other GSI techniques with somewhat different mechanisms include horizontal and V-shaped soft buried barriers (Nappa et al. 2016; Flora et al. 2018), sliding effects of stone pebble layer (Banović et al. 2019), as well as a periodic foundation for creating effective attenuation zones (Shi et al. 2014; Cheng et al. 2020). A review of a range of other GSI (or soil improvement) techniques can be found in Ortiz-Palacio et al. (2015).

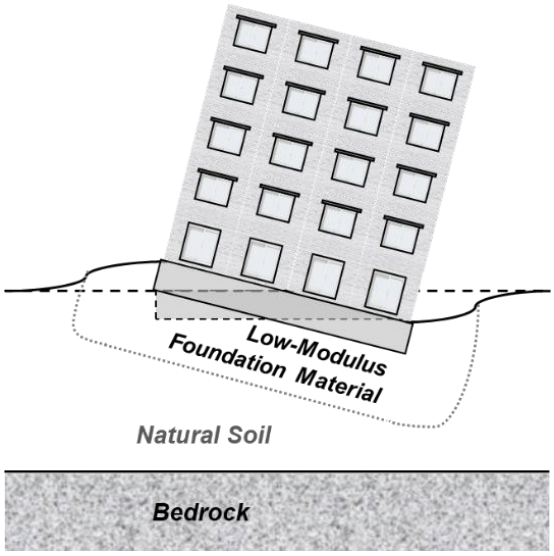

Figure 1 Schematic diagram illustrating the (magnified) augmented rocking mechanism of geotechnical seismic isolation (GSI) system based on well-controlled low-modulus foundation material.

The effectiveness of GSI system based on RSM (abbreviated as GSI-RSM system) in reducing structural demand has been demonstrated in numerous numerical studies (Mavronicola et al. 2010; Tsang et al. 2012; Abdelhaleem et al. 2013; Abdullah and Hazarika 2015; Pitilakis et al. 2015; Anbazhagan et al. 2016; Brunet et al. 2016; Forcellini 2017; Nanda et al. 2018; Dhanya et al. 2020), whilst experimental investigation has been limited. Small-scale 1-g shaking table tests were conducted on lumped-mass models sitting on mixtures of sand and shredded rubber tyre (Xiong and Li 2013; Bandyopadhyay et al. 2014). It was found that GSI-RSM system could achieve a greater response reduction with higher percentage of rubber, thicker layer of RSM or at higher shaking levels. Shimamura (2012) has developed two composite materials based on mixing soil-cement slurry with ductile nylon fibres and tyre rubber chips or high-damping rubber chips for backfilling around the peripheral of the foundation. It was found from a small-scale 1-g shaking table test that structural response was reduced, whilst foundation rocking was increased. Recently, Tsiavos et al. (2019) have performed both direct shear test and small-scale 1-g shaking table test to investigate the kinetic friction and sliding potential of granular sand-rubber layer with various interface materials. Sliding was found to occur at high shaking levels with peak ground acceleration (PGA) exceeding 0.4 g.

On the other hand, Kaneko et al. (2013) have conducted online pseudodynamic test (also known as hybrid simulation) to investigate the effectiveness of layers of tyre chip-sand mixtures in reducing seismic response and excess pore-water pressure. The effectiveness was found to increase as tyre chip content increased. Also, field tests were conducted on the performance of RSM-filled sleeved piles (Komakpanah and Khoshay 2015) and trench barriers (Mahdavisefat et al. 2018). These studies suggested that an increase in rubber content would enhance energy absorption capability.

More experimental research efforts are needed for an improved understanding of the behaviour and mechanism of GSI system, as identified as one of the three key aspects of future development (Tsang and Pitilakis 2019). As GSI system involves the interaction between superstructure, foundation system, RSM and subsoil under strong earthquake shaking, physical testing on scaled models in a 1-g environment may not be ideal in reflecting the actual nonlinear response behaviour of subsoil and RSM. Hence, this study aims to investigate the performance of GSI system via geotechnical centrifuge testing, which can accurately replicate prototype stresses and strains of subsurface materials by creating an artificial gravitational acceleration. Whilst centrifuge tests were conducted for soft buried barriers (Nappa et al. 2016) and rocking isolation systems (Loli et al. 2014, Pelekis et al. 2018), this article presents the first dynamic centrifuge testing on GSI-RSM system.

2 EXPERIMENTAL SET-UP

2.1 Geotechnical Centrifuge Facility

The testing was conducted at the Centrifuge Modelling Laboratory at National Central University (NCU) in Taiwan, which is internationally recognised and representative of the Asia-Pacific region (Kutter et al. 2018). The centrifuge apparatus has a nominal radius of 3 m and a one-dimensional servo-hydraulic-controlled earthquake shaker that is assembled on its swing basket as shown in Fig. 2(a). The shaker has a maximum payload of 400 kg at a maximum acceleration field of 80 g which is corresponding to a maximum nominal force of ±53.4 kN. The maximum table displacement is ±6.4 mm with a maximum input frequency of 250 Hz. The payload mounting area of the shaker is 1000 mm (length) × 550 mm (width) (Hung and Liao 2020). The container used is a laminar box as shown in Fig. 2(b). The inner dimensions are 711 mm (length) × 356 mm (width) × 353 mm (height), and the net weight of the empty box is 84 kg.

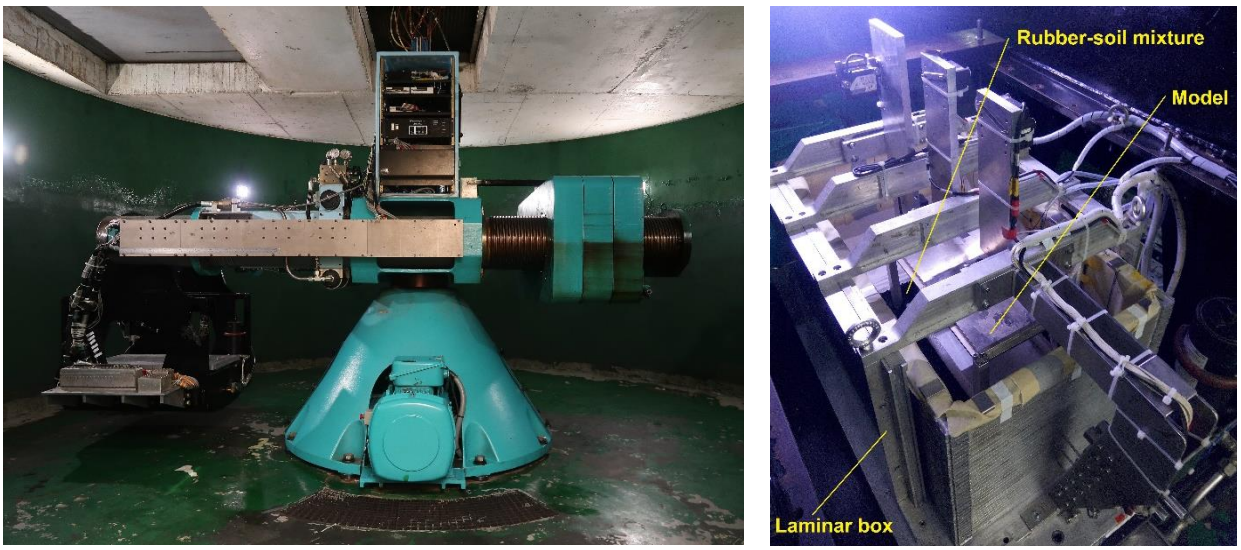

(a) (b)

Figure 2 (a) Overview of the geotechnical centrifuge facility at National Central University (NCU) in Taiwan, and (b) the laminar box with the test model mounted in the swing basket.

2.2 Geometry of Building Model

In this study, a realistic five-story moment resisting frame building was considered for guiding the design of the test model. Assuming that the prototype building is 15 m tall with masses uniformly distributed along the height, the effective height of the corresponding idealised single-degree-of-freedom (SDOF) model can be taken as 10 m. A rectangular floor plan of 18 m by 12 m was considered. A shallow embedment depth of 1 m was assumed, which includes a 0.5 m thick raft footing.

Scaling laws define the relationships between the dimensions and response parameters of the centrifuge model and those of the prototype. Descriptions of the scaling laws adopted in this study can be found in Garnier et al. (2007). A centrifugal acceleration field of 50 g was chosen for the test.

A single-story frame structure model with a height, h_{eff}, of 200 mm (measured from the base of footing to the centre of structure's mass) and a plan of 360 mm by 240 mm was designed to capture the key dynamic properties and response characteristics of the prototype five-story building. Realistic lateral stiffness of the structure was provided by the columns at the four corners. The self-weight of the building was represented by the roof slab, whilst lumped masses were added onto the roof slab as the live loads, which also allowed the flexibility to adjust the total mass of the structure in order to achieve the desired natural period of the model. Note that 10 mm thick plastic wall barriers of 30 mm tall were provided around the structure to avoid materials getting into the building model during the test.

2.3 Instrumentation for Measuring Performance Indicators

The array of accelerometers designed for measuring performance indicators and the responses at other key locations is shown in Fig. 3. The total acceleration response of the lumped masses at the roof of the frame, $\ddot{X}^T$, is indicative of the equivalent seismic force experienced by the building, hence, an accelerometer (A7) was attached at the top of the lumped masses. A series of other accelerometers were deployed at various locations for providing extra information of the response characteristics of the system.

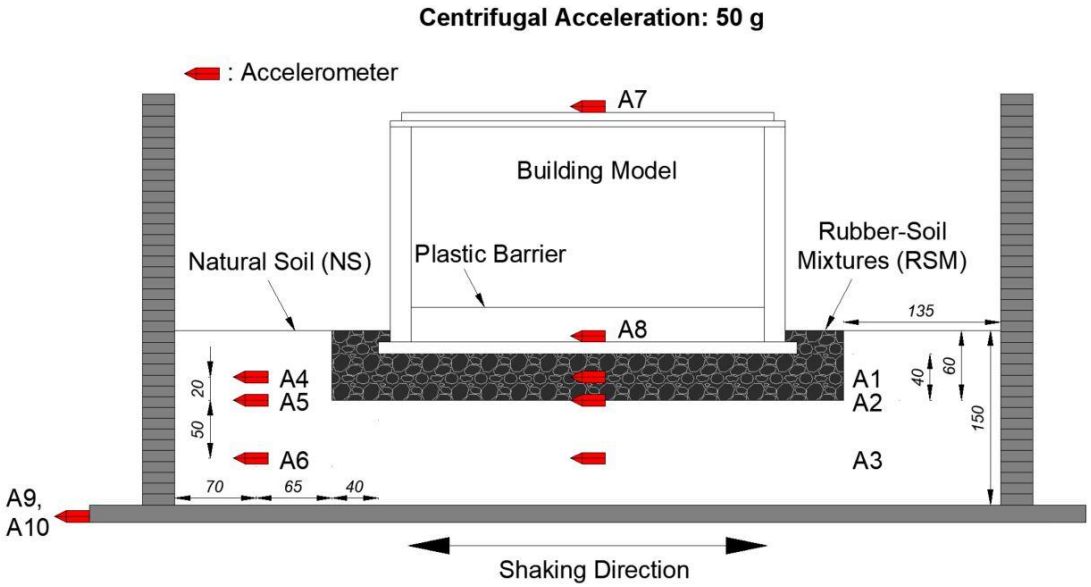

Figure 3 Centrifuge test set-up with the array of accelerometers (dimensions in mm).

Another key performance measure of GSI system is the reduction of inter-story drift response of the structure, x_{str}, which is representative of the damage potential as commonly adopted in a displacement-based seismic assessment/design framework, such as the one presented in Menegon et al. (2019). This is essentially the actual deformation of the columns without the rigid-body rotational component due to foundation rotation. An indirect method using basic structural dynamics theory was adopted to obtain x_{str} based on the total acceleration responses recorded at the roof, $\ddot{X}^T$. Eq. (1) shows the governing equation of the dynamic equilibrium of the idealised SDOF system as shown in Fig. 4(a):

$$m_{str}\ddot{X}^T + c_{str}\dot{x}_{str} + k_{str}x_{str} = 0 \quad (1)$$

where m_{str} is the mass of the equivalent lumped mass, c_{str} and k_{str} are respectively the damping coefficient and lateral stiffness of the system, and

$$\ddot{X}^T = \ddot{x}_{str} + \ddot{x}_f + h_{eff}\ddot{\theta}_f + \ddot{x}_g \quad (2)$$

in which, the four terms on the right-hand side are the second derivatives of the individual displacement response components as defined in Fig. 4(b). Noted that capital letter "*X*" is used to indicate measured responses.

In order to calculate x_{str} from $\ddot{X}^T$ based on Eq. (1), the first derivative of x_{str} is needed. Hence, an iterative process is required to achieve equality in Eq. (1). The first estimate of x_{str} can be made by ignoring the damping term as it is expected to be small.

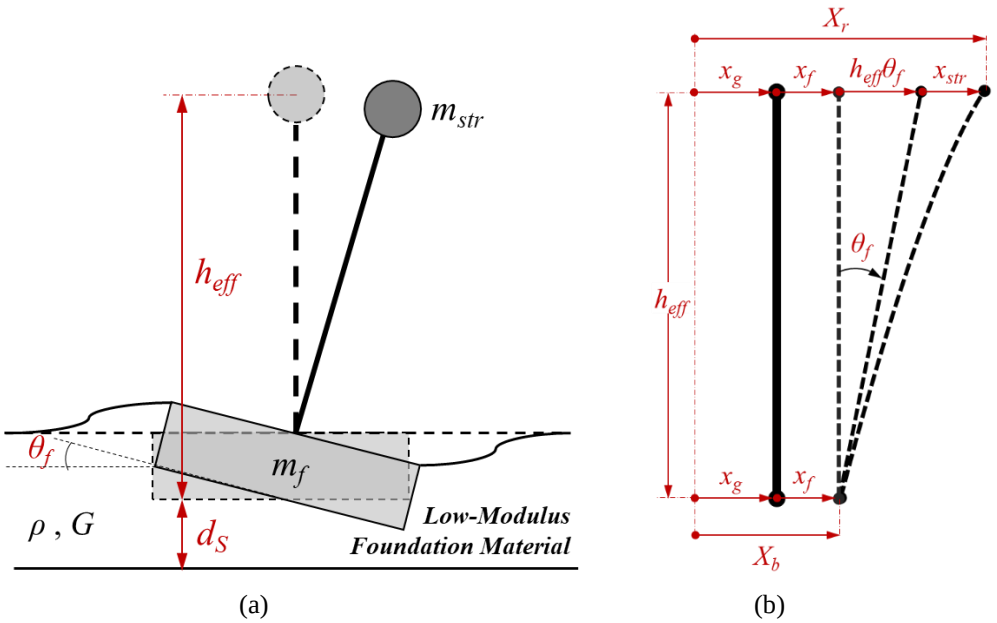

Figure 4 (a) Idealised model of a building, sitting on a shallow foundation underneath by low-modulus foundation material with controllable properties, and (b) the definitions of response parameters.

3 OVERVIEW OF EXPERIMENTAL PROGRAMME

3.1 GSI System Design

Earlier studies found that GSI system with a thicker layer of low-modulus RSM foundation material can give greater reduction of structural demand, in terms of acceleration and inter-story drift (Tsang et al. 2012; Pitilakis et al. 2015; Brunet et al. 2016). Whilst a thicker layer also consumes a larger amount of scrap tyres, which is attractive from the waste recycling perspective, there are concerns regarding the possibly high cost of deep excavation with lateral support and the lack of relevant site formation skills in underprivileged regions. Meanwhile, it was shown in recent analytical studies that a layer of 2–3 m is sufficient for achieving significant response reduction (Brunet et al. 2016; Tsang and Pitilakis 2019). Hence, a thin layer of d_S = 2 m underneath and surrounding the raft footing was specified in this study, which is equivalent to 40 mm in model scale, as shown in Fig. 3. The entire RSM layer is assumed to be located above the groundwater table.

The mechanical properties of RSM significantly depend on the effective confining pressure, proportion between rubber and soil, and the relative size between soil and rubber particles ($D_{50,s}/D_{50,r}$). Based on the design self-weight and imposed loads on the prototype five-story frame building, an overburden pressure of around 58 kPa has to be mimicked in the centrifuge immediately underneath the raft foundation. This was achieved by adjusting the amount of lumped masses placing on the roof of the model building with the consideration of the target fundamental natural period of the building model and the masses of other components of the frame model and sensors.

Three foundation materials with different proportion between rubber and soil were considered in this study, namely natural soil (NS) (without rubber) (Fig. 5(a)), RSM with 30% rubber by weight (RSM-30%) (Fig. 5(b)) and RSM with 40% rubber by weight (RSM-40%). It was found in previous studies (Sheikh et al. 2013; Mashiri et al. 2015; Disfani et al. 2017) that the skeleton of RSM is formed by both soil and rubber particles when rubber content is between 10–18% and 30–35% by weight. Hence, RSM-30% would behave as a true mixture, whilst RSM-40% is expected to exhibit rubber-like behaviour.

(a) (b)

Figure 5 Foundation materials in soil container: (a) Natural soil (NS), (b) rubber-soil mixtures (RSM) with 30% rubber by weight (RSM-30%) backfilled in designated region underneath and surrounding the raft footing of building model.

The prototype NS material selected was clean gravel (with less than 5% fines), which was poorly graded with $D_{50,s}$ of 7.3 mm. The $D_{50,r}$ of rubber granules in RSM was 3.1 mm, hence, the ratio $D_{50,r}/D_{50,s}$ equals to 0.425. As the ratio of the smaller footing dimension (240 mm in model scale) to the average grain size ($D_{50,s}$ = 7.3 mm) is at least 32, statistically significant number of particles are involved at the contact interface. Hence, prototype grain size could be used in centrifuge testing (Alnuaim et al. 2015; Bolton et al. 1999; Kutter 1995; Taylor 1994). The target density of each of the three foundation materials is given in Table 1. They were filled into the laminar box layer by layer with a target relative density of 70%. It is noted that the effective confining pressure varied slightly amongst cases with NS, RSM-30% and RSM-40% because a small amount of these materials was placed on top of the peripheral of the raft footing (outside the plastic wall barriers).

Table 1 Small-strain shear modulus (G_0, MPa) and density (ρ, kg/m^3) of foundation materials.

Material	Rubber content (% by weight)	Density (kg/m^3)	G_0 calculated based on SASW method	G_0 predicted based on Anastasiadis et al. (2012)
Natural Soil	0	1680	78	106
RSM-30%	30	1160	5.0	5.8
RSM-40%	40	1050	3.7	2.8

3.2 Small-strain Shear Modulus

The method of the spectral analysis of surface waves (SASW) was adopted to estimate the small-strain shear modulus of the foundation materials. The SASW method is based on the dispersion of Rayleigh wave, of which the velocity is reasonably close to that of shear wave for the range of Poisson's ratio expected in this study. This method was adopted by Murillo et al. (2009) and Taeseri et al. (2018) to assess shear wave velocity and shear modulus of soils near the surface in centrifuge model.

Before and between earthquake scenarios in each flight, a small-amplitude 3-Hz (in prototype scale) sinusoidal wave was applied by the shaker. To apply the SASW method, the time histories recorded by the two accelerometers (A1, A2) underneath the raft footing, $a_1(t)$ and $a_2(t)$, were firstly converted to the frequency domain, $A_1(f)$ and $A_2(f)$, through Fast Fourier Transform. The phase difference, ϕ, between the Rayleigh wave motions recorded at the two receivers can be obtained as a function of frequency, f:

$$\phi = arctan\left[\frac{Im(S_{A_1A_2})}{Re(S_{A_1A_2})}\right] \quad (3)$$

in which $S_{A_1A_2}$ is the cross-spectrum between the two motions. Based on the phase difference function, the travelling time for each frequency between the two receivers can be calculated by:

$$t(f) = \frac{\phi(f)}{2\pi f} \quad (4)$$

Finally, shear (or Rayleigh) wave velocity, V_S, can be calculated from the travelling time and the distance between the two receivers, d_r. Small-strain shear modulus, G_0, is then calculated from the shear wave velocity and the density, ρ.

$$V_S(f) = \frac{d_r}{t(f)} \quad (5)$$

$$G_0(f) = \rho[V_S(f)]^2 \quad (6)$$

The dispersion points are considered valid if the coherence values are higher than 0.95, according to Oppenheim and Schafer (1989). This is a measure of the quality of coherence of the two signals at various frequencies, with a maximum value of 1.0. In this study, a coherence value higher than 0.95 can generally be achieved for frequency below 3 Hz (in prototype scale). The results at the frequency with a higher coherence have been reported in Table 1, along with the predicted values based on Anastasiadis et al. (2012). It is noted that the differences of the actual small-strain shear modulus amongst the three foundation materials are not as much as predicted. Having said that, the two sets of values are considered reasonably close with each other given the high variability of soil properties and the possible errors with the SASW method and the predictive equations in Anastasiadis et al. (2012).

It is clear from Table 1 that the small-strain shear modulus of RSM is significantly lower than that of NS. This has raised a concern whether initial settlement would be excessive or not. Extensive research in the past decade has improved the understanding of the mechanical properties of RSM. It is expected that the GSI-RSM foundation layer can be properly designed, constructed and compacted to achieve desirable properties. Initial settlements exist but at a controllable level.

3.3 Input Ground Motions

Strong ground motion time histories recorded in four major earthquakes were mimicked by the shaker in the centrifuge in this study. The basic information of the earthquakes is summarised in Table 2. The values of peak ground acceleration (PGA) of the original records vary from 0.35 g to 1.78 g.

Table 2 Details of earthquake ground motion records used in the centrifuge.

	Northridge, U.S.	Algarrobo, Chile	El Salvador	Imperial Valley, U.S.
Local Date	17 Jan 1994	3 Mar 1985	13 Jan 2001	18 May 1940
Magnitude, M_w	6.7	8.0	7.6	6.9
Recording Station	Tarzana	Llolleo	La Libertad	El Centro
Unscaled PGA (g)	1.78	0.45	0.72	0.35
Target PGA (g)	0.45	0.45	0.65	0.65

In order to investigate the effects of shaking levels on the performance of GSI-RSM system, two levels of PGA, namely 0.45 g and 0.65 g, were selected as the targets, given the upper limit of around 0.7 g that the shaker in the centrifuge can possibly produce. All four earthquake excitations were applied successively in each flight, whilst several attempts were made to achieve the target PGA levels by adjusting the input voltage to the shaker. Results from two earthquake scenarios with PGA = 0.45 g and the other two scenarios with PGA = 0.65 g will be presented in Section 4. Fig. 6 shows the 5%-damped elastic acceleration response spectra for the four input motions that were recorded at the base of the laminar box (A9 and A10 shown in Fig. 3). The variation of responses at different periods

can clearly be seen, which is indicative of the distinctive frequency contents of the selected ground motion records. Hence, the robustness of GSI-RSM system with respect to ground motions of different frequency contents can be examined.

Meanwhile, progressive stiffening of the foundation materials through the four selected cases is considered insignificant as a series of prior shaking events with PGA up to at least 0.4 g was applied, which could serve as a soil compaction procedure. It is also common to apply a series of earthquake excitations in each flight of a centrifuge test (Loli et al. 2014, Pelekis et al. 2019).

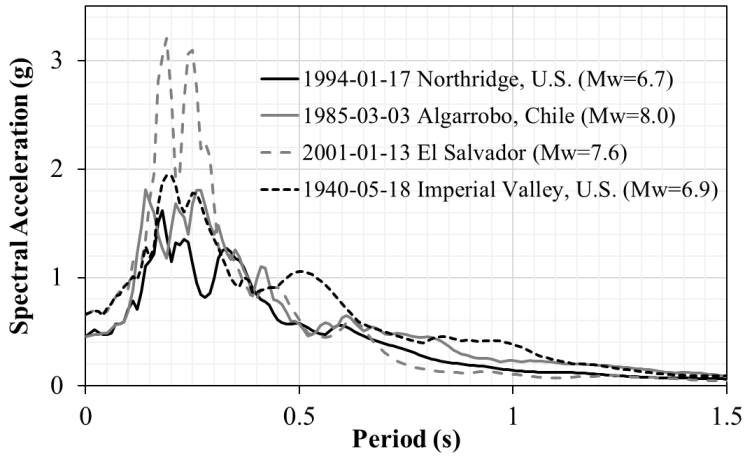

Figure 6 5%-damped elastic acceleration response spectra for the input ground motions recorded at the base of the laminar box.

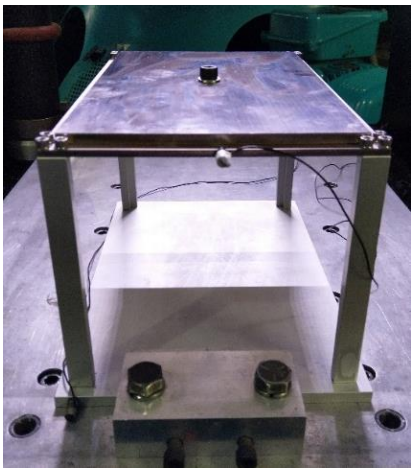

Figure 7 Fixed-base structure model for free vibration test.

3.4 Characteristics of Soil-foundation-structure Systems

The single-story frame structure can be taken as a SDOF model of which the fundamental natural period can be calculated based on the total mass at the top and the lateral stiffness provided by the columns. According to the Australian Standard AS1170.4-2007, the fundamental natural period of five-story moment resisting concrete and steel frame building is in the order of 0.71 s and 1.05 s respectively. Hence, a fundamental natural period of 0.85 s was set as the target for the design of the frame in prototype scale. This is corresponding to a fundamental natural period of 0.017 s for the test model. As the lateral stiffness of the frame model was 928 kN/m and the mass of the fixed roof slab was 2.97 kg (in model scale), a lumped mass of 3.78 kg (in model scale) had to be added on top of the roof slab in order to achieve the target fundamental natural period.

Prior to the actual testing, free vibration test was conducted for checking the fundamental natural period and damping ratio of the fixed-base frame model, as shown in Fig. 7. The building model alone was fixed onto a platform and an initial motion was induced by gently striking the top of the frame model with a hammer. Acceleration response at the top of the frame was recorded, from which the corresponding Fourier amplitude spectrum can be calculated. It is found that the predominant frequency of the acceleration response is 1.18 Hz (in prototype scale). It was therefore confirmed that the target fundamental natural period of the fixed-base frame model has been achieved. The damping ratio was found by the method of logarithmic decrement.

On the other hand, the fundamental natural period and damping ratio of the coupled soil-structure system with the frame model founded on NS, RSM-30% or RSM-40% can be obtained from the free vibrations after each earthquake event. Acceleration response at the top of the frame model was recorded, such that the flexible-base natural period of the coupled soil-structure system can be obtained from the corresponding Fourier amplitude spectrum. The key results are summarised in Table 3.

Table 3 Fundamental natural period (in prototype scale) and damping ratio measured from free vibrations of the fixed-base structure and the flexible-base system with different foundation materials.

	Fixed-base structure	Flexible-base system		
Foundation material	–	NS	RSM-30%	RSM-40%
Fundamental natural period (s)	0.85	0.88	1.11	1.25
Natural period ratio	–	1.0	1.26	1.42
Damping ratio (%)	0.95	1.8	3.0	5.9

4 RESULTS AND DISCUSSION

4.1 Structural Demand Reduction

Fig. 8 shows the time histories of the total acceleration response recorded at the roof of the frame (A7), $\ddot{X}^T$ (in prototype scale), for the cases when the structure was sitting on NS and RSM-30%, respectively, whilst Fig. 9 shows the time histories of the inter-story drift (deformation) demand on the columns, x_{str} (in prototype scale). The results for GSI-RSM-40% are not included into the plots, as it would be hard to distinguish them from others visually. It is, however, noted that the reduction rates for GSI-RSM-40% are consistently higher. The peak absolute values and the corresponding percentage reduction of the two demand parameters for all cases are summarised in Table 4. It is seen that GSI-RSM-30% can reduce structural demand by 34–50% (42% on average), whilst the use of a higher proportion of rubber in RSM (i.e. 40% by weight) can result in a demand reduction by 43–59% (50% on average).

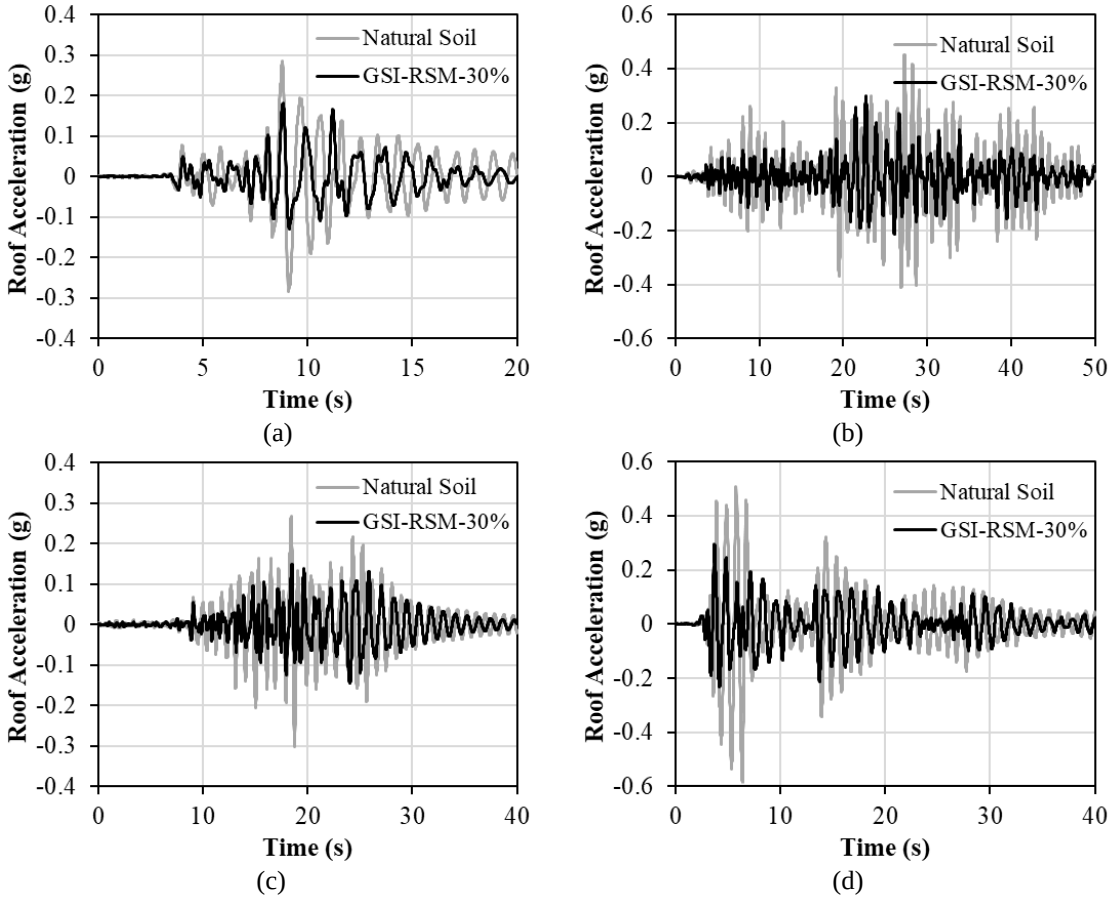

Figure 8 Time histories of the total acceleration response recorded at the roof of the frame, $\ddot{X}^T$ (in prototype scale): (a) 1994 Northridge earthquake, (b) 1985 Algarrobo earthquake, (c) 2001 El Salvador earthquake, and (d) 1940 Imperial Valley earthquake.

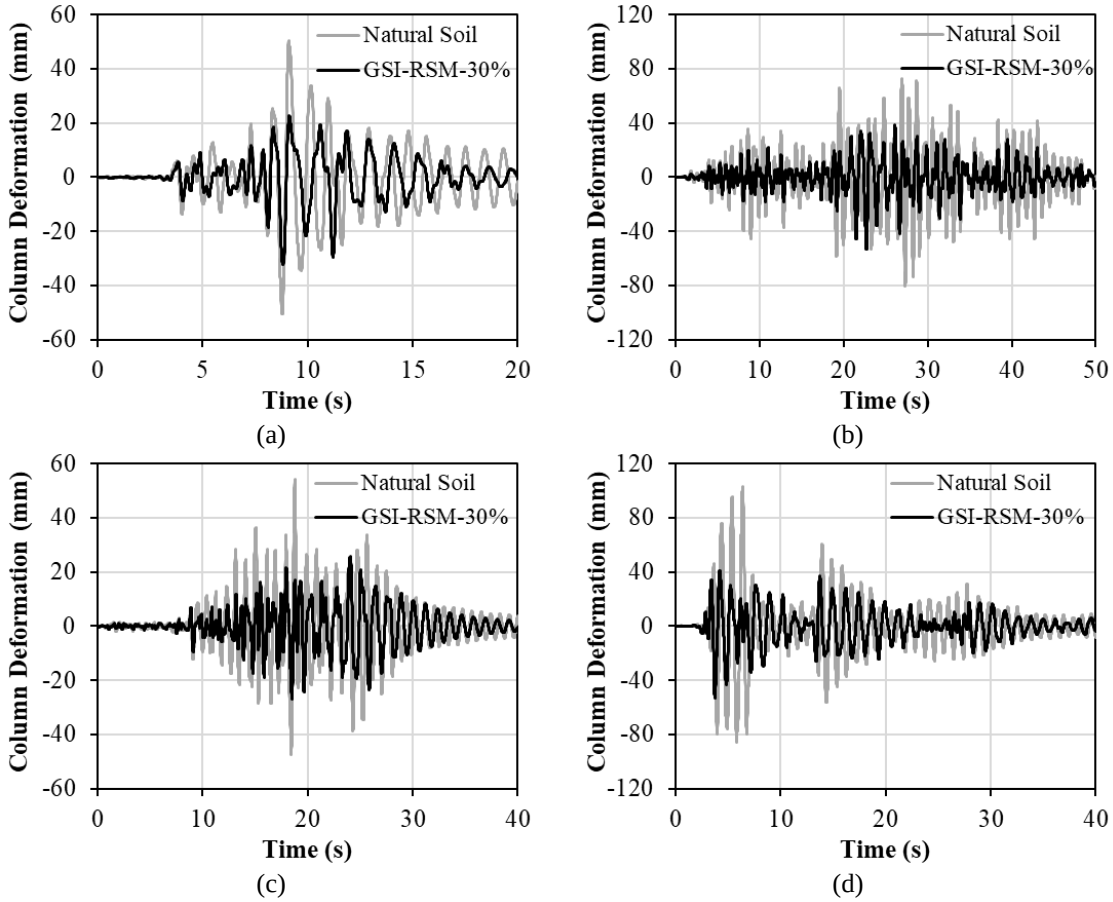

Figure 9 Time histories of the inter-story drift (deformation) demand on the columns, x_{str} (in prototype scale): (a) 1994 Northridge earthquake, (b) 1985 Algarrobo earthquake, (c) 2001 El Salvador earthquake, and (d) 1940 Imperial Valley earthquake.

Table 4 Peak absolute values and percentage reduction of the total acceleration response recorded at the roof of the frame, $\ddot{X}^T$ (g) and the inter-story drift (deformation) demand on the columns, x_{str} (mm) (in prototype scale).

Peak Absolute Value of	Northridge, U.S.	Algarrobo, Chile	El Salvador	Imperial Valley, U.S.
$\ddot{X}^T$ – Natural Soil	0.28	0.45	0.30	0.58
$\ddot{X}^T$ – GSI-RSM-30%	0.18	0.30	0.15	0.30
	–36%	*–34%*	*–51%*	*–49%*
$\ddot{X}^T$ – GSI-RSM-40%	0.16	0.25	0.13	0.28
	–43%	*–46%*	*–56%*	*–52%*
x_{str} – Natural Soil	51	80	54	103
x_{str} – GSI-RSM-30%	32	53	27	53
	–36%	*–34%*	*–51%*	*–49%*
x_{str} – GSI-RSM-40%	28	43	22	48
	–44%	*–47%*	*–59%*	*–53%*

The reduction rates obtained from this study are generally lower than the 50–60% reduction obtained from analytical modelling, such as in Brunet et al. (2016) and Tsang and Pitilakis (2019). There are two possible reasons for that: (i) The actual small-strain modulus of the gravel used for natural soil (NS) in the experiment is significantly lower than that adopted in the analytical studies, which were estimated based on Anastasiadis et al. (2012) as reported in Table

1. Hence, the difference in the modulus between NS and RSM would be smaller, which in turn, led to slightly closer structural responses and lower reduction rates. (ii) The lower shaking level applied in the centrifuge, which resulted in higher dynamic modulus and lower rocking rotations, and in turn, less prominent isolation effects. In fact, a closer look at the results shown in Table 4 reveals that the average reduction rate is 40% for Northridge earthquake and Algarrobo earthquake when PGA were 0.45 g, whereas an average of 52% demand reduction was resulted for El Salvador earthquake and Imperial Valley earthquake when PGA were 0.65 g.

It is noteworthy that this study is based on only one test model with specific dimensions and structural configuration. Different structural models need to be considered in future studies. For example, one may postulate that the building height-to-width aspect ratio could influence the performance of GSI-RSM system. Whilst the numerical study conducted by Tsang et al. (2012) revealed only a slight drop in demand reduction when aspect ratio increases, the effects of this important parameter deserve further investigation.

On the other hand, it can be seen from the results that the reduction rates are mostly consistent between the total acceleration response and the column deformation demand. It seems to indicate a rather direct proportionality between the two response parameters. Referring back to Eq. (1) and the relevant discussion in Section 2.3, it is likely because the damping term is insignificant, and hence, the following approximation becomes valid:

$$x_{str} \cong -\frac{m_{str}}{k_{str}} \ddot{X}^T \tag{7}$$

This has been confirmed by the recorded data that a difference of less than half a per cent of the peak absolute response values would be resulted from this approximation. In fact, as there are phase differences of π/2 between the damping term and the other two terms in Eq. (1), local maxima and minima of the inertial and stiffness terms occur when the damping term is close to zero. Hence, it is acceptable to ignore the damping term, provided that the peak response values are the most important performance indicators.

4.2 Foundation Response Amplification

The isolation mechanism of GSI system is founded on the reduced horizontal stiffness of foundation soil layer, i.e. RSM in this study, and the lower Young's modulus that leads to the reduction of rocking stiffness of the soil-foundation-structure interaction system. This is analogous to a combination of the traditional seismic isolation system with the use of rubber bearings and the emerging concept of rocking isolation. The seismic demand can be redistributed between superstructure and foundation material layer, such that the structural demand can be reduced. An important indicator is an increase in both horizontal displacement and rotation response of foundation, which has clearly been shown through analytical modelling in Tsang and Pitilakis (2019). This study intends to provide experimental evidence of this important phenomenon.

The horizontal displacement of the foundation slab relative to input (ground) displacement, x_f, was obtained through a standard procedure (Kutter et al. 2018). This was calculated by firstly subtracting the acceleration at the foundation (A8) from the acceleration at the base of the laminar box (A9, A10), and then a double integration with respect to time. A 0.2 Hz (in prototype scale) high pass filter was applied before and after each integration to remove unwanted drift. The rotation response of the foundation can be calculated from Eq. (8), in which X_r and X_b are the displacement in the horizontal direction at the roof and the foundation slab, respectively, which were obtained from double integration of the acceleration records (A7, A8) with respect to time.

$$\theta_f = \frac{X_r - X_b - x_{str}}{h_{eff}} \tag{8}$$

Figs. 10 and 11 show the time histories of the horizontal relative displacement (in prototype scale) and rotation response of the foundation slab, respectively, for the non-isolated (NS) case and the GSI-RSM system with 30% rubber content by weight. It is shown that both response parameters were increased. Also, it is worth noting that these foundation response parameters were increased even more for RSM material with 40% rubber content. The low-stiffness RSM foundation layer can offer a similar function as rubber bearings, to a lesser extent though, whilst rocking

isolation mechanism can be augmented with reversible foundation deformations due to the elasticity of RSM material. It is postulated that structures with higher height-to-width aspect ratio could experience larger rotations.

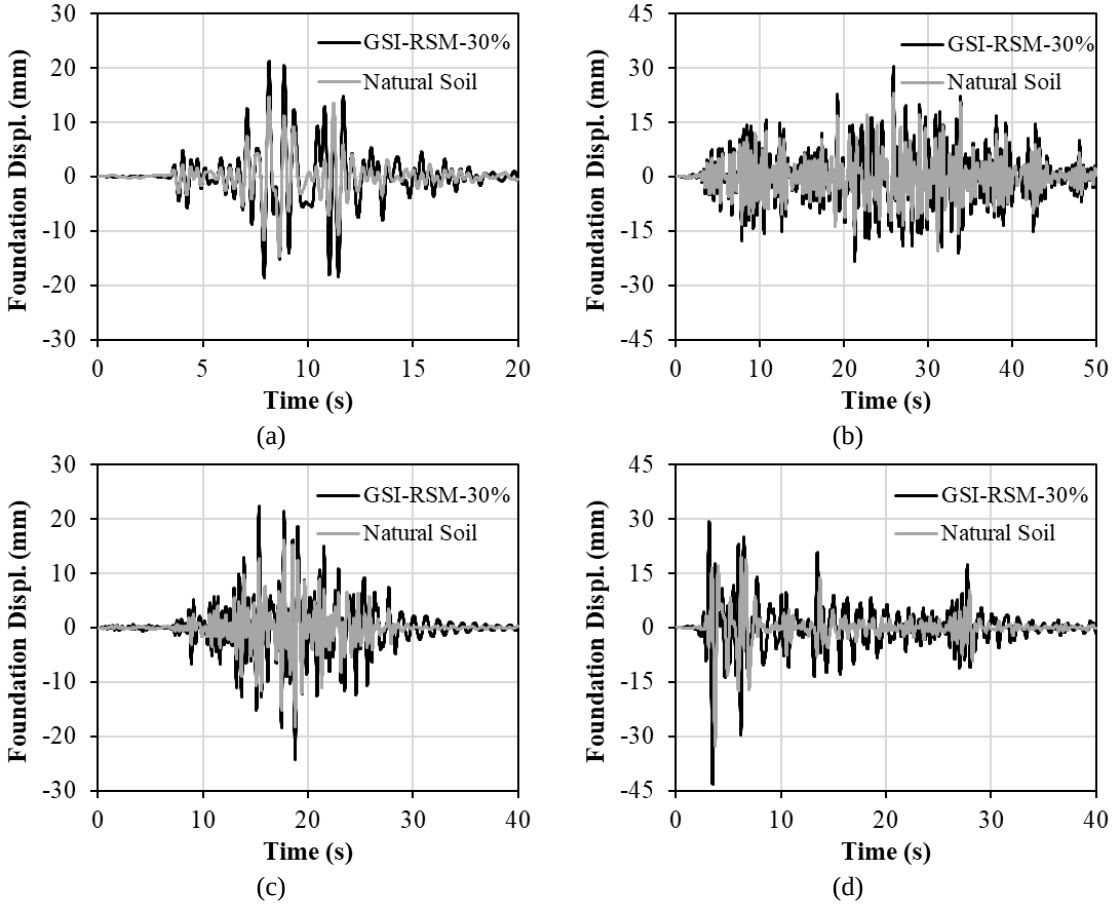

Figure 10 Time histories of the horizontal displacement response of the foundation slab relative to the base of the laminar box, x_f (in prototype scale): (a) 1994 Northridge earthquake, (b) 1985 Algarrobo earthquake, (c) 2001 El Salvador earthquake, and (d) 1940 Imperial Valley earthquake.

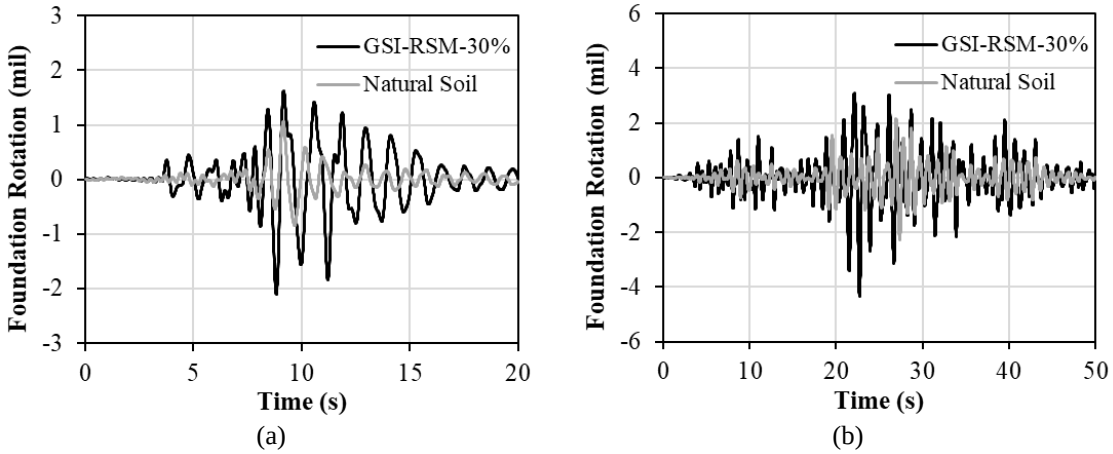

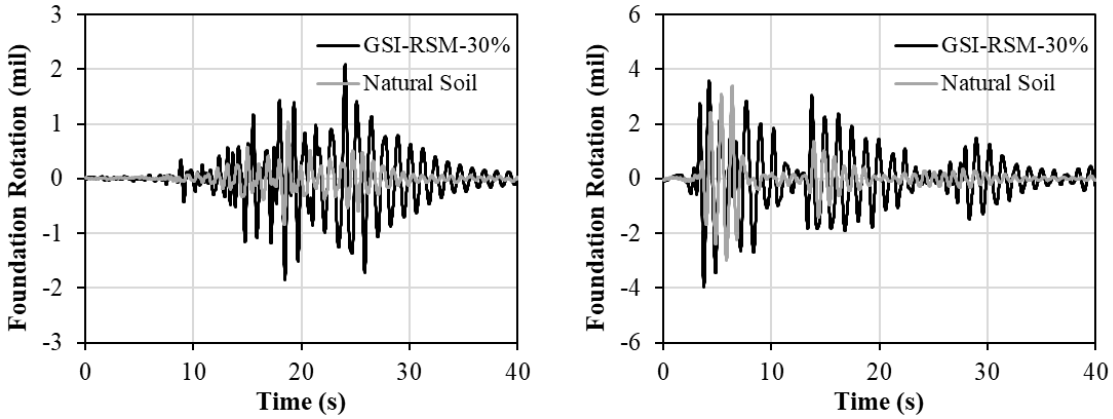

Figure 11 Time histories of the rotation response of the foundation, θ_f (in unit of milliradian, i.e. mil): (a) 1994 Northridge earthquake, (b) 1985 Algarrobo earthquake, (c) 2001 El Salvador earthquake, and (d) 1940 Imperial Valley earthquake.

The elastic response behaviour of RSM foundation layer can be shown by the hysteresis in the form of a moment-rotation plot. The bending moment at the base of the structure including the additional moment due to P-Delta effects can be calculated by Eq. (9).

$$M_b = k_{str} x_{str} h_{eff} + m_{str} g\left(x_{str} + h_{eff}\theta_f\right) \tag{9}$$

Fig. 12 shows the moment-rotation response behaviour of the foundation that was sitting on NS and RSM-30% respectively. The bending moment was reduced, and the foundation rotation was increased for the GSI system. It is clearly evidenced that the rocking stiffness of the GSI-RSM system was significantly reduced, which has facilitated rocking isolation. Importantly, the thin and nearly linear hysteretic loops, even at larger rotation (or deformation), illustrate the elasticity of the foundation layers. Hence, the undesirable residual ground deformation (defined by Anastasopoulos et al. (2010) as soil failure or yielding and by Gajan et al. (2005) as permanent settlement, rotation or sliding that may cause damage to the building) could be avoided or minimised. This can arguably be an advantage of the proposed GSI system over the conventional rocking isolation (below foundation) approach.

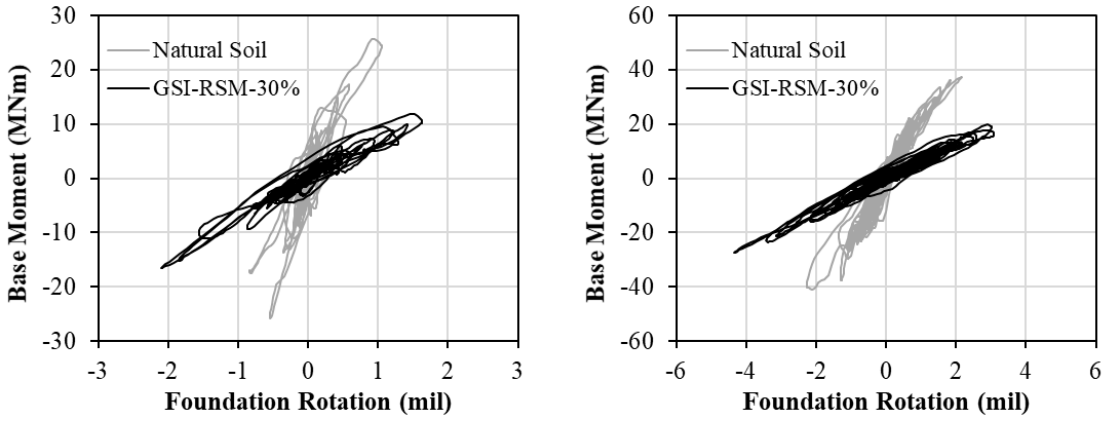

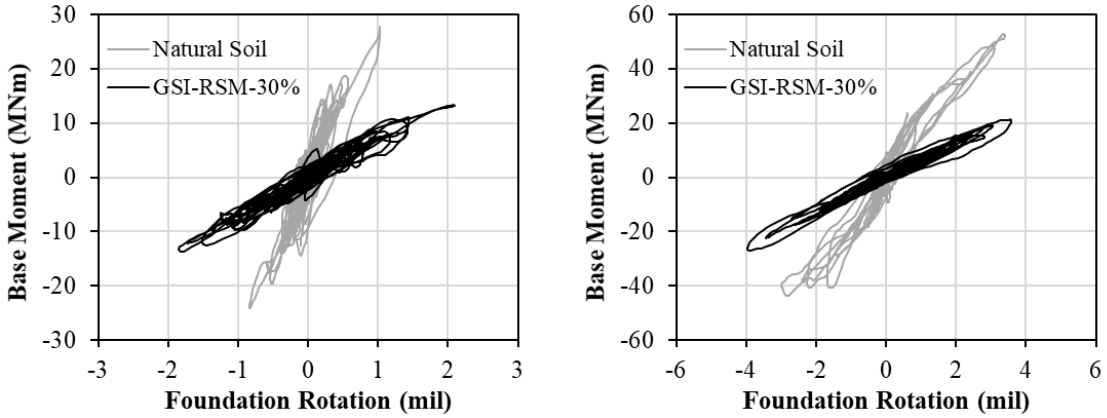

Figure 12 Moment-rotation response of the foundation (in prototype scale): (a) 1994 Northridge earthquake, (b) 1985 Algarrobo earthquake, (c) 2001 El Salvador earthquake, and (d) 1940 Imperial Valley earthquake.

4.3 Shear Behaviour of Foundation Materials

Apart from the change in foundation rocking stiffness at system level as discussed in the previous sub-section, the change in stiffness and the hysteretic response behaviour can also be investigated at material level. In this sub-section, the stress-strain response histories of the foundation materials are calculated and compared, from which the shear modulus at the largest strain can be obtained.

Theoretically, the shear stress τ and shear strain γ at time t at any depth z measured from the bottom of the raft foundation can be calculated based on the governing equations of one-dimensional shear wave propagation:

$$\frac{\partial \tau(z,t)}{\partial z} = \rho \frac{\partial^2 u(z,t)}{\partial t^2} \tag{10}$$

$$\gamma(z,t) = \frac{\partial u(z,t)}{\partial z} \tag{11}$$

where u is the horizontal displacement and ρ is the mass density of the foundation material.

The time-varying shear stress representative of the mid-depth of the RSM layer, $z = d_S/2$, and the time-varying average shear strain across the RSM layer can be computed based on an approximation of Eq. (10) and (11) as proposed by Zeghal and Elgamal (1994), which was also used by Ghosh and Madabhushi (2007) to evaluate the stress and strain of soil underneath a raft foundation:

$$\tau\left(\frac{d_S}{2}, t\right) = \rho d_S \frac{\ddot{u}\left(\frac{d_S}{2}, t\right) + \ddot{u}(0,t)}{4} \tag{12}$$

$$\gamma(t) = \frac{u(d_S,t) - u(0,t)}{d_S} \tag{13}$$

However, Brennan et al. (2005) commented that reliable surface acceleration is rarely available in centrifuge testing, a linear fit was recommended between the top pair of accelerometers (A1, A2), which can then be extrapolated to the surface. A 0.2 Hz (in prototype scale) high pass filter was applied to the acceleration time series $\ddot{u}(t)$ (Kutter et al. 2018) before integrating with respect to time twice to obtain displacement time history $u(t)$.

Fig. 13(a) shows the full shear stress-strain response history at the mid-depth of each foundation material, namely NS, RSM-30% and RSM-40%, during 2001 El Salvador earthquake as an illustration. The loop with the largest average (of peak positive and peak negative) strain from each case was extracted and presented in Fig. 13(b). The secant shear modulus, G, of each loop has also been calculated and annotated in the plot. The key results are summarised in Table 5 along with the corresponding shear modulus reduction ratio, G/G_0, calculated from the test data, in comparison with the ratio corresponding to the respective shear strain value estimated based on Senetakis et al. (2012).

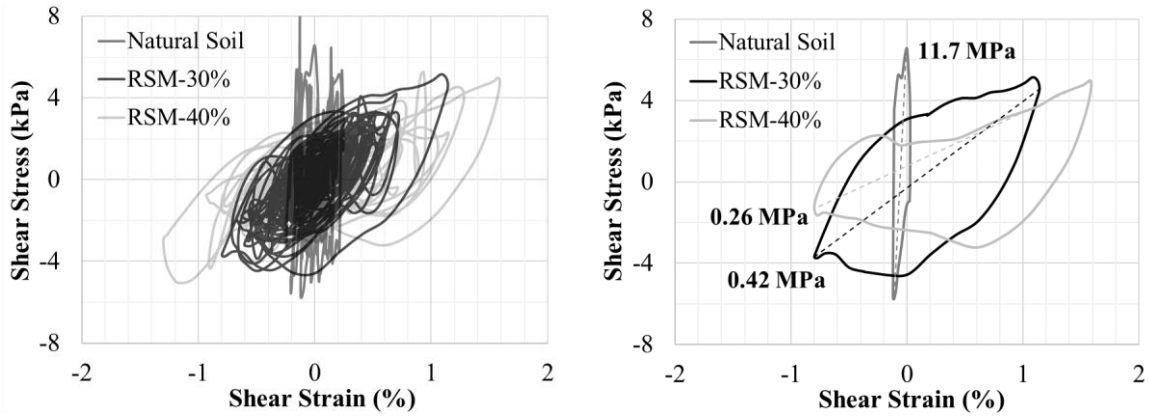

Figure 13 Shear stress-strain response of each foundation material during 2001 El Salvador earthquake: (a) full response history, and (b) the loop with the largest average strain of which the secant shear modulus is annotated.

Table 5 Secant shear modulus (G, MPa) at the largest average strain and the corresponding shear modulus reduction ratio (G/G_0) of foundation materials.

Material	Largest average shear strain (%)*	G at the largest average strain	G/G_0 based on test data	G/G_0 estimated based on Senetakis et al. (2012)
Natural Soil	0.17	11.7	0.15	0.21
RSM-30%	0.97	0.42	0.084	0.094
RSM-40%	1.19	0.26	0.070	0.105

* average of peak positive and peak negative strain

An interesting finding is that although the shear stress-strain response of RSM shows hysteretic energy dissipation, the moment-rotation response at system level that is primarily based on compressional action during foundation rocking is nearly elastic with little hysteretic energy dissipation. A possible explanation is that rubber (and RSM) can be deformed rather easily in shear due to the low shear modulus (G), whilst axial compression is harder due to their high Poisson's ratio and constrained modulus (M). This may explain the low level of nonlinearity in the moment-rotation behaviour at system level and the small foundation rotations in Fig. 12. A further evidence is that, due to the higher M/G ratio of RSM than NS, the hysteretic loops of RSM are even thinner and more linear than those of NS as shown in Fig. 12. Also, the amount of rotations of the two cases is rather comparable, whilst the shear strain of RSM is much larger as shown in Fig. 13. Further research on this phenomenon is needed.

4.4 Energy Dissipation

Apart from evaluating the performance of the GSI-RSM system based on percentage reduction of peak structural demand, an energy approach can be adopted to quantify the relative amount of energy dissipation amongst various modes of response. When seismic wave energy gets into the structure-foundation system, part of the energy is dissipated through structural (column) deformation, whilst part of it is radiated from the structure to the subsoil through sliding and rocking. The time-varying kinetic energy being dissipated through the three response modes, E_{str}, E_f and E_θ, respectively, can be computed using Eq. (14)–(16).

$$E_{str}(t) = \frac{1}{2} m_{str} \dot{x}_{str}(t)^2 \tag{14}$$

$$E_f(t) = \frac{1}{2} \left(m_{str} + m_f\right) \dot{x}_f(t)^2 \tag{15}$$

$$E_\theta(t) = \frac{1}{2} \left(I_{str} + I_f\right) \dot{\theta}_f(t)^2 \tag{16}$$

I_{str} and I_f are, respectively, the mass moment of inertia of the structure and that of the foundation about the centroidal axis across the base of the foundation:

$$I_{str} = m_{str} {h_{eff}}^2 \tag{17}$$

$$I_f = m_f \left(\frac{{R_\theta}^2}{4} + \frac{{h_f}^2}{3} \right) \tag{18}$$

in which h_f is the thickness of the raft footing and R_θ is the equivalent radius of the foundation for rocking motions that can be computed by equating the second moment of area about the centroidal axis, e.g. for a rectangular foundation with dimension $2L \times 2B$:

$$R_\theta = \sqrt[4]{\frac{16BL^3}{3\pi}} \tag{19}$$

The time series of the accumulative energy dissipation of the individual response modes, normalised to the total amount of kinetic energy, during 1994 Northridge earthquake are plotted in Fig. 14 for the non-isolated (natural soil) case and the GSI-RSM system with 30% rubber content by weight. When the structure is sitting on natural soil, over 70% of the seismic energy is dissipated in the structure. Meanwhile, a quarter of the energy is radiated through sliding, whilst rocking is minimal. Experimental data show that the accumulative energy being dissipated in the isolated structure has been significantly reduced by 65%, whereas the energy being radiated from the structure to the subsoil through sliding and rocking has been tremendously increased by 120% and 470% respectively. This illustrates the favourable effects of seismic soil-foundation-structure interaction being exploited by the GSI-RSM system. The augmented rocking mechanism has particularly been highlighted by the enormous increase in the amount of energy being radiated through rocking.

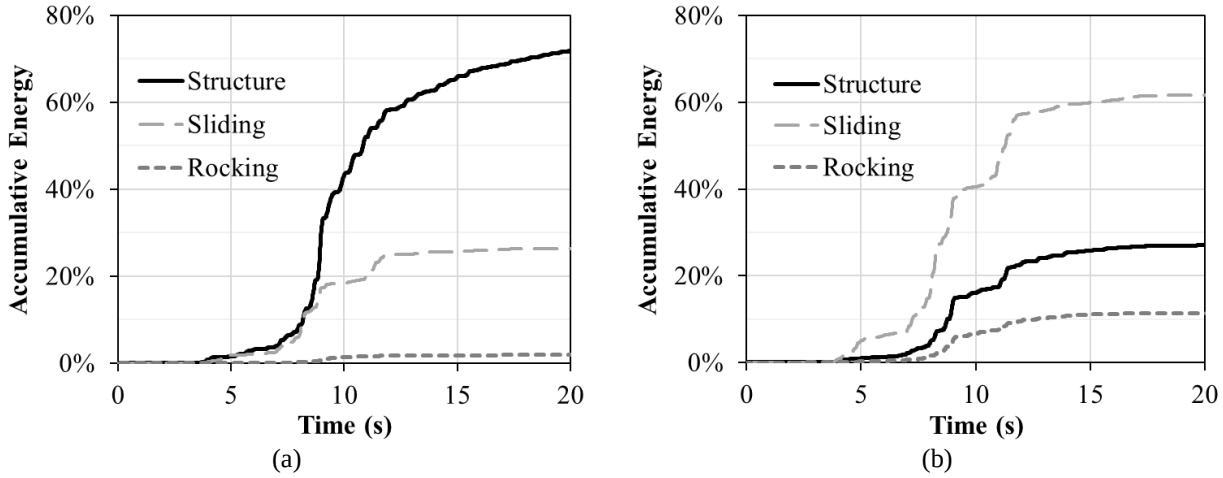

Figure 14 Accumulative energy dissipated in the structure and the energy radiated from the structure to the subsoil through sliding and rocking, respectively, normalised to the total amount of kinetic energy, during

1994 Northridge earthquake: (a) non-isolated (natural soil) case, and (b) GSI-RSM system with 30% rubber content by weight.

5 CONCLUSIONS

This paper presents the first geotechnical centrifuge testing on an emerging earthquake protection system, namely geotechnical seismic isolation (GSI) that is founded on the use of rubber-soil mixtures (RSM) as a well-controlled low-modulus foundation material. This technique involves a reduced horizontal stiffness of RSM layer and the lower modulus of RSM that reduces rocking stiffness, with an aim to exploit the beneficial role of soil-foundation-structure interaction in structural demand reduction.

It is evidenced from the test results presented in this paper that the isolation effect could be achieved by redistributing the seismic demand on the whole soil-foundation-structure system to the RSM foundation layer, such that the structural demand can be reduced by as much as 40–50%. This phenomenon has been confirmed in the dynamic centrifuge tests that both the horizontal and rotation responses of the foundation slab have been amplified in the GSI-RSM system. Also, the total energy being dissipated in the isolated structure has been reduced by over 60%, whereas the total energy being radiated from the structure to the subsoil through sliding and rocking has been tremendously increased.

The increase in horizontal response of the foundation is analogous to the large shear displacement that is experienced by rubber bearings during an earthquake, whereas the increased yet reversible rotation response of the foundation due to reduced rocking stiffness leads to an augmented rocking mechanism, which is a unique feature of GSI-RSM system. Importantly, the elasticity of the properly designed RSM foundation layer as observed in the tests can avoid soil failure/yielding and minimise the undesirable residual ground deformation due to rotation and sliding.

ACKNOWLEDGMENTS

The financial support from the Bushfire and Natural Hazards Cooperative Research Centre [Project A9] of the Australian Government is acknowledged.

DATA AVAILABILITY STATEMENT

The data that support the findings of this study are available from the corresponding author upon reasonable request.

REFERENCES

Abdelhaleem AM, El-Sherbiny RM, Lotfy H, Al-Ashaal AA. Evaluation of Rubber/Sand Mixtures as Replacement Soils to Mitigate Earthquake Induced Ground Motions. Proceedings of the 18th International Conference on Soil Mechanics and Geotechnical Engineering, Paris, France, 2013.

Abdullah A, Hazarika H. Improvement of shallow foundation using non-liquefiable recycle materials. Japanese Geotechnical Society Special Publication 2015;2(54):1863-1867.

Alnuaim AM, El Naggar H, El Naggar MH. Performance of micropiled raft in sand subjected to vertical concentrated load: centrifuge modeling. Can Geotech J 2015;52:33–45.

Anastasiadis A, Senetakis K, Pitilakis K. Small-strain shear modulus and damping ratio of sand-rubber and gravel-rubber mixtures. Geotech Geol Eng 2012;30(2):363–382.

Anastasopoulos I, Gazetas G, Loli M, Apostolou M, Gerolymos N. Soil failure can be used for seismic protection of structures. Bull. Earthquake Eng. 2010;8(2):309–326.

Anastasopoulos I, Kourkoulis R, Gelagoti F, Papadopoulos E. Rocking response of SDOF systems on shallow improved sand: An experimental study. Soil Dyn. Earthquake Eng. 2012, 40, 15–33.

Anastasopoulos I, Loli M, Georgarakos T, Drosos V. Shaking table testing of rocking-isolated bridge pier on sand. J. Earthquake Eng. 2013, 17(1), 1–32.

Anbazhagan P, Manohar DR, Divyesh R. Low cost damping scheme for low to medium rise buildings using rubber soil mixtures. Japanese Geotechnical Society Special Publication 2016;3(2):24-28.

Argyroudis S, Palaiochorinou A, Mitoulis S, Pitilakis D. Use of rubberised backfills for improving the seismic response of integral abutment bridges. Bulletin of Earthquake Engineering 2016;14(12):3573–3590.

AS 1170.4-2007 Structural design actions, Part 4: Earthquake actions in Australia, Standards Australia, Sydney, NSW.

Bandyopadhyay S, Sengupta A, Reddy GR. Natural base isolation system for earthquake protection. Current Science 2014;107(6):1037-1043.

Banović I, Radnić J, Grgić N (2019) Geotechnical Seismic Isolation System Based on Sliding Mechanism Using Stone Pebble Layer: Shake-Table Experiments. Shock and Vibration; Article ID 9346232.

Bolton MD, Gui MW, Garnier J, Corté JF, Bagge G, Laue J, Renzi R. Centrifuge cone penetration tests in sand, Géotechnique 1999;49(4):543–552.

Brennan AJ, Thusyanthan NI, Madabhushi SPG. Evaluation of Shear Modulus and Damping in Dynamic Centrifuge Tests. Journal of Geotechnical and Geoenvironmental Engineering 2005;131(12):1488-1497.

Brunet S, de la Llera JC, Kausel E. Non-linear modeling of seismic isolation systems made of recycled tire-rubber. Soil Dynamics and Earthquake Engineering 2016;85:134–145.

Cheng, Z., Shi, Z., Palermo, A., Xiang, H., Guo, W., Marzani, A. Seismic vibrations attenuation via damped layered periodic foundations. Engineering Structures 2020;211, Article no. 110427.

Dhanya JS, Boominathan A, Banerjee S. Response of low-rise building with geotechnical seismic isolation system. Soil Dynamics and Earthquake Engineering 2020;136, Article no. 106187.

Disfani MM, Tsang HH, Arulrajah A, Yaghoubi E. Shear and Compression Characteristics of Recycled Glass-Tire Mixtures. ASCE Journal of Materials in Civil Engineering 2017;29(6), Article no. 06017003.

Flora A, Lombardi D, Nappa V, Bilotta E. Numerical Analyses of the Effectiveness of Soft Barriers into the Soil for the Mitigation of Seismic Risk. Journal of Earthquake Engineering 2018;22(1):63-93.

Forcellini D. Assessment on geotechnical seismic isolation (GSI) on bridge configurations. Innovative Infrastructure Solutions 2017;2:9. DOI: 10.1007/s41062-017-0057-8

Gajan S, Phalen JD, Kutter BL, Hutchinson TC, Martin G. Centrifuge modeling of load deformation behavior of rocking shallow foundations. Soil Dyn. Earthquake Eng. 2005;25(7–10):773–783.

Gajan S, Kutter BL. Capacity, settlement and energy dissipation of shallow footings subjected to rocking. J. Geotech. Geoenviron. Eng. 2008;134:8(1129):1129–1141.

Garnier J, Gaudin C, Springman SM, Culligan PJ, Goodings DJ, Konig D, et al. Catalogue of scaling laws and similitude questions in geotechnical centrifuge modelling. Int J Phys Model Geotech 2007;8(3):1–23.

Ghosh B, Madabhushi SPG. Centrifuge modelling of seismic soil structure interaction effects. Nuclear Engineering and Design 2007;237(8):887–896.

Hazarika H, Kohama E, Sugano T. Underwater shake table tests on waterfront structures protected with tire chips cushion. Journal of Geotechnical and Geoenvironmental Engineering, ASCE 2008;134(12):1706–1719.

Hung WY., Liao TW. (2020) LEAP-UCD-2017 Centrifuge Tests at NCU. In: Kutter B., Manzari M., Zeghal M. (eds) Model Tests and Numerical Simulations of Liquefaction and Lateral Spreading. Springer, Cham.

Kaneko T, Orense RP, Hyodo M, Yoshimoto N. Seismic response characteristics of saturated sand deposits mixed with tire chips. Journal of Geotechnical and Geoenvironmental Engineering, ASCE 2013;139(4):633-643.

Karatzia X, Mylonakis G. Geotechnical isolation of pile-supported bridge piers using EPS geofoam. Proceedings of the 16th World Conference on Earthquake Engineering, Santiago, Chile, January 9-13, 2017.

Komakpanah A, Khoshay AH. A new seismic isolation system: sleeved-pile with soil-rubber mixture. International Journal of Civil Engineering, Vol. 13, No. 2, Transaction B: Geotechnical Engineering 2015:124-132.

Kutter BL. Recent advances in centrifuge modeling of seismic shaking. International Conferences on Recent Advances in Geotechnical Earthquake Engineering and Soil Dynamics 1995; 4.

Kutter, B., Carey, T., Hashimoto, T., Zeghal, M., Abdoun, T., Kokalli, P., Madabhushi, G., Haigh, S., Hung, W.-Y., Lee, C.-J., Iai, S., Tobita, T., Zhou, Y. G., Chen, Y., & Manzari, M. T. (2018). LEAP-GWU-2015 experiment specifications, results, and comparisons. Soil Dynamics and Earthquake Engineering, 113, 616–628.

Lee JH, Salgado R, Bernal A, Lovell CW. Shredded tires and rubber-sand as lightweight backfill. Journal of Geotechnical and Geoenvironmental Engineering, ASCE 1999;125(2):132–141.

Loli M, Knappett JA, Brown MJ, Anastasopoulos I, Gazetas G. Centrifuge modeling of rocking-isolated inelastic RC bridge piers. Earthquake Engineering and Structural Dynamics 2014;43(15):2341-2359.

Mahdavisefat E, Salehzadeh H, Heshmati AA. Full-scale experimental study on screening effectiveness of SRM-filled trench barriers. Géotechnique 2018;68(10):869-882.

Mashiri MS, Vinod JS, Sheikh MN, Tsang HH. Shear Strength and Dilatancy Behaviour of Sand-Tire Chip Mixtures. Soils and Foundations 2015;55(3):517-528.

Mavronicola E, Komodromos P, Charmpis DC. Numerical investigation of potential usage of rubber–soil mixtures as a distributed seismic isolation approach. Proceedings of the 10th International Conference on Computational Structures Technology, Valencia, Spain, September 14–17, 2010.

Menegon, S.J., Tsang, H.H., Lumantarna, E., Lam, N.T.K., Wilson, J.L., Gad, E.F. (2019). Framework for Seismic Vulnerability Assessment of Reinforced Concrete Buildings in Australia. Australian Journal of Structural Engineering, 20(2):143-158.

Mitoulis SA, Palaiochorinou A, Georgiadis I, Argyroudis S. Extending the application of integral frame abutment bridges in earthquake-prone areas by using novel isolators of recycled materials. Earthquake Engineering and Structural Dynamics 2016;45(14):2283-2301.

Murillo CA, Thorel L and Caicedo B (2009) Spectral analysis of surface waves method to assess shear wave velocity within centrifuge models. Journal of Applied Geophysics 68(2):135–145.

Nanda RP, Dutta S, Khan HA, Majumder S. Seismic Protection of Buildings by Rubber-Soil Mixture as Foundation Isolation. International Journal of Geotechnical Earthquake Engineering 2018;9(1):99-109.

Nappa V, Bilotta E, Flora A, Madabhushi SPG. Centrifuge modelling of the seismic performance of soft buried barriers. Bulletin of Earthquake Engineering 2016, DOI: 10.1007/s10518-016-9912-9

Oppenheim, A., Schafer, R., 1989. Discrete-Time Signal Processing. PrenticeHall, Englewood Cliffs, NJ.

Ortiz-Palacio S, Ibáñez SJ, López-Ausín V, Porres JA. Earthquake Vulnerability and the State-of-the-Art of Hybrid Structural Reinforcement and Soil Improvement Methods for Non-Engineered Structures. Proceedings of the 6th International Conference on Earthquake Geotechnical Engineering, Christchurch, New Zealand, 1-4 November 2015.

Pelekis I, Madabhushi GSP, DeJong MJ. Seismic performance of buildings with structural and foundation rocking in centrifuge testing. Earthquake Engineering and Structural Dynamics 2018;47(12):2390–2409.

Pelekis I, Madabhushi GSP, DeJong MJ. Soil behaviour beneath buildings with structural and foundation rocking. Soil Dynamics and Earthquake Engineering 2019;123:48–63.

Pitilakis K, Karapetrou S, Tsagdi K. Numerical investigation of the seismic response of RC buildings on soil replaced with rubber–sand mixtures. Soil Dynamics and Earthquake Engineering 2015;79:237–252.

Senetakis K, Anastasiadis A, Pitilakis K. Dynamic properties of dry sand/rubber (SRM) and gravel/rubber (GRM) mixtures in a wide range of shearing strain amplitudes. Soil Dynamics and Earthquake Engineering 2012;33:38–53.

Sheikh MN, Mashiri MS, Vinod JS, Tsang HH. Shear and Compressibility Behaviors of Sand-Tire Crumb Mixtures. ASCE Journal of Materials in Civil Engineering 2013;25(10):1366-1374.

Shi Z, Cheng Z, Xiang H. Seismic isolation foundations with effective attenuation zones. Soil Dynamics and Earthquake Engineering 2014;57:143-151.

Shimamura A. Study on Earthquake Response Reduction by Improved Composite Geo-material using Rubber Chips and Fibrous materials (translated from Japanese). PhD Thesis, Osaka University, Japan, 2012. (in Japanese)

Taeseri D, Laue J, Martakis P, Chatzi E and Anastasopoulos I (2018) Static and dynamic rocking stiffness of shallow footings on sand: centrifuge modelling. International Journal of Physical Modelling in Geotechnics 18(6): 315–339.

Taylor RN. Centrifuges in modelling: principles and scale effects. Chapter 2 in Geotechnical Centrifuge Technology, (Ed.) Taylor R.N., 1st Edition, CRC Press, London, 1994, 296 pp.

Terzi NU, Erenson C, Selçuk ME. Geotechnical properties of tire-sand mixtures as backfill material for buried pipe installations. Geomechanics and Engineering 2015;9(4):447-464.

Tsang HH. Seismic isolation by rubber–soil mixtures for developing countries. Earthquake Engineering and Structural Dynamics 2008;37(2):283–303.

Tsang HH. Geotechnical seismic isolation. In: Earthquake Engineering: New Research, New York, U.S.: Nova Science Publishers Inc; 2009, p. 55–87.

Tsang HH. Uses of scrap rubber tires. In: Rubber: Types, Properties and Uses, New York, U.S.: Nova Science Publishers Inc; 2012, p. 477-492.

Tsang HH, Pitilakis K. Mechanism of geotechnical seismic isolation system: Analytical modeling. Soil Dynamics and Earthquake Engineering 2019;122:171–184.

Tsang HH, Lo SH, Xu X, Sheikh MN. Seismic isolation for low-to-medium-rise buildings using granulated rubber–soil mixtures: numerical study. Earthquake Engineering and Structural Dynamics 2012;41:2009–2024.

Tsang HH, Lam JYK, Yaghmaei-Sabegh S, Lo SH. Protecting underground tunnel by rubber–soil mixtures. Proceedings of the 7th International Conference on Lifeline Earthquake Engineering, ASCE-TCLEE, Oakland, California, U.S., June 28 – July 1, 2009.

Tsiavos, A., Alexander, N.A., Diambra, A., Ibraim, E., Vardanega, P.J., Gonzalez-Buelga, A., Sextos, A. A sand-rubber deformable granular layer as a low-cost seismic isolation strategy in developing countries: Experimental investigation. Soil Dynamics and Earthquake Engineering 2019;125, Article no. 105731.

Xiao M, Bowen J, Graham M, Larralde J. Comparison of Seismic Responses of Geosynthetically Reinforced Walls with Tire-Derived Aggregates and Granular Backfills. Journal of Materials in Civil Engineering, ASCE 2012;24(11):1368-1377.

Xiong W, Li Y. Seismic isolation using granulated tire–soil mixtures for less-developed regions: experimental validation. Earthquake Engineering and Structural Dynamics 2013;42:2187–2193.

Zeghal, M., and Elgamal, A.-W. (1994). Analysis of site liquefaction using earthquake records. J. Geotech. Eng., 120(6), 996–1017.